Modification effects of colloidal nanoSiO2 on cement hydration and its gel property

Pengkun Hou [a,b,*], Shiho Kawashima [b], Deyu Kong [b,c], David J. Corr [b], Jueshi Qian [a], Surendra P. Shah [b]

[a] College of Materials Science and Engineering, Chongqing University, Chongqing 400045, China
[b] Department of Civil and Environmental Engineering, Northwestern University, Evanston, IL 60208, USA
[c] College of Architecture and Civil Engineering, Zhejiang University of Technology, Hangzhou 310014, China

ABSTRACT

To understand the effects of colloidal nanoSiO2 (CNS) on cement hydration and gel properties in the early and later age, hydration heat, calcium morphology, hydroxide content, non-evaporable water (NEW) content and nanoscale mechanical properties were measured. Some comparison studies were conducted on silica fume (SF) paste, as well. Results revealed that the accelerating effect of CNS on hydration in the early age is achieved by the acceleration of cement dissolution and hydrate nucleation on reacted nano-SiO2 particles. Although cement hydration can be greatly accelerated by CNS in the early age, its later age hydration is hindered. The NEW content of CNS-added paste experiences a higher rate of increase initially, but gradually becomes smaller than that of the control paste due to changes in the gel structure, making NEW content an unsuitable method for monitoring the hydration of CNS-added paste. However, nanoindentation results revealed that CNS modifies the gel structure to increase the high-stiffness C–S–H gel content.

© 2012 Elsevier Ltd. All rights reserved.

1. Introduction

Nanotechnology has been introduced to cement and concrete research because it can achieve a stronger and more durable concrete [1,2]. As the most widely used nanomaterial for cement/concrete-engineering, nanoSiO2 has been studied intensively [3–13]. It has been widely reported that nanoSiO2 addition can greatly improve properties of cementitious materials [3–10]. Jo et al. [6] reported that 6% nanoSiO2 can improve the compressive strength of concrete by 152% and 142% at 7 and 28 days, respectively; Li [7] found that 5% nanoSiO2 can improve compressive strength by 17.5% at 28 day; Gaitero et al. [9] revealed reduced calcium leaching of nanoSiO2-added cement pastes. They ascribed it to densification of the paste, transforming of Portlandite into C–S–H gel by means of pozzolanic reaction and modification of the internal structure of C–S–H gel, all of which make the cement paste more stable and more strongly bonded [10].

Property evolution of nanoSiO2-added cementitious materials can be reflected by the effects of nanoSiO2 on cement hydration, gel property modification, and pore structure refinement [3,13–16]. Results have shown that the strength enhancing effect of nanoSiO2 in the early age is related to its hydration acceleration effect, but its effects in the later age have rarely been reported. For the compressive strength enhancing effect of nanoSiO2, it was found to be more pronounced in the early age, while rate of strength gain can be lower than the control in the later ages [8]. The difference in the strength gain evolution at the early and later ages requires that the effect of nanoSiO2 on cement hydration in both ages be investigated.

Thus, in this study, cement hydration characteristics in the presence of nanoSiO2 in the early and later ages, including hydration acceleration rate, hydration acceleration mechanisms, cement hydration degree, and the resulting gel properties were investigated. All of these results help to provide a comprehensive explanation for the modification effects of nanoSiO2 on cementitious materials. To make a comparison, effects of silica fume on cement hydration were also studied.

2. Experimental

2.1. Materials and mix proportions

A type I Portland cement with a Blaine fineness of 385 m^2/kg was used in this study. To facilitate a homogeneous distribution of nanoSiO2 in cement paste, colloidal nanoSiO2 (CNS), instead of nanoSiO2 powder, was used. Sodium stabilized CNS with an average particle size of 10 nm (CNS-10) produced by the sol–gel technique was used. The basic properties were provided by the manufacturer [17]. A silica fume was used for a comparison study with CNS. The physiochemical properties of the raw materials are given in Tables 1 and 2.

* Corresponding author at: College of Materials Science and Engineering, Chongqing University, Chongqing 400045, China.
E-mail address: pkhou@163.com (P. Hou).

CNS	Average particle size (nm)	SiO$_2$ content (wt.%)	pH
CNS-10	10	>99	10.5

Table 2
Physiochemical properties of raw materials.

Materials	Type I cement	Silica fume
SiO$_2$	20.2	90.1
Al$_2$O$_3$	4.7	0.6
Fe$_2$O$_3$	3.3	2.0
SO$_3$	3.3	–
CaO	62.9	0.5
MgO	2.7	5.1
LOI	1.1	1.0
Total	98.2	99.3
Fineness as surface area (m^2/kg)	380	21 000

The transmission electron microscopy (TEM) images of CNS-10 in Fig. 1 shows that most of the CNS particles are well-dispersed but some agglomeration can still occur. The near-perfect sphericity of the SF particles is evident (Fig. 1) and the spheres are quite smooth, with no obvious surface morphology. It is also apparent that SF is composed of various sized particles ranging from several to dozens of nanometers. XRD spectra shown in Fig. 2 indicate the amorphous feature of both pozzolans. A similar full width at half maximum indicates that the two materials have a comparable crystallinity.

2.2. Sample preparation

Unless stated otherwise, cement pastes mixed with and without 5% CNS/SF at a w/b ratio of 0.4 were prepared and investigated throughout this study. Samples were demolded 1 day after casting and were cured in saturated lime solution at room temperature until testing.

For the pozzolanic activity study, 20 g of chemical grade calcium hydroxide (CH) were mixed with 5 g of CNS/SF at a w/b of 2 to simulate a cement-CNS/SF system. It was assumed that 20 g of CH can be generated by 100 g of cement [18]. After mixing, samples were sealed in plastic vials. The CH content at different ages were determined by a TGA technique.

2.3. Test methods

2.3.1. Hydration heat

The hydration temperature of each paste was measured by a semi–adiabatic calorimeter to assess the effect of CNS/SF on the hydration heat of cement. Samples were prepared at a w/b ratio of 0.4, with 100 g of cement and mixing water at a temperature of 27 °C. Mixes were cast in ∅5.08 cm × 10.16 cm plastic cylinders within 3 min after initial cement and water contact. The sample was then covered, placed in the calorimeter, and the temperature of the sample was recorded every 3 min for 20 h.

2.3.2. Morphology

Hitachi S-4800 FE-SEM and Hitachi S-3400 (equipped with backscatter electron detector) were used to analyze the morphology of the cement paste. Small fractured samples or powder samples at very early hydration ages were soaked in acetone to stop hydration and dried at 80 °C for 2 h. Then the sample was coated with 20 nm of gold to make it conductive.

2.3.3. CH content

Thermogravimetric analysis (TGA, TGA/sDTA 851) was carried out to measure CH content. The weight loss between 440 °C and 510 °C was considered to be the decomposition of CH. Before measuring, samples were oven – dried at 105 °C for 4 h. CH contents were calculated on the ignited basis at 950 °C for 30 min.

2.3.4. Non-evaporable water (NEW) content

At the end of curing, the core of the sample was crushed into small pieces and immediately immersed in acetone to stop hydration, as well as to minimize carbonization. Before measuring the NEW content, samples were oven – dried at 105 °C for 4 h and then ground to pass the 100 mesh size (ca. 150 μm) sieve. The NEW content was measured as the weight loss of the sample between 105 °C and 950 °C. After firing at 950 °C for half an hour, the sample weight loss was measured and NEW was calculated on the ignited basis at 950 °C for 30 min of the sample using Eq. (1). For each mix, three samples (ca. 2 g of each) were measured and the average value was taken as the representative value.

$$\text{NEW}\% = 100 \times \left[\frac{w_{105°C} - w_{950°C}}{w_{950°C}} - (f_{cem} \times \text{loss}_{cem} + f_{FA} \times \text{loss}_{FA} + f_{CNS/SF} \times \text{loss}_{CNS/SF}) \right] \tag{1}$$

where w is the sample weight, f is the weight percentage of material.

2.3.5. Nanoscale mechanical property

To determine the effect of CNS on the nanoscale mechanical properties of cement paste, a statistical nanoindentation technique was applied, through which the intrinsic gel modifying effect of CNS can be shown. During this test, a load of 1000 μN was applied with a triangle diamond Berkovich indenter with a total included angle of 142.3° to make an indent on the surface of the sample.
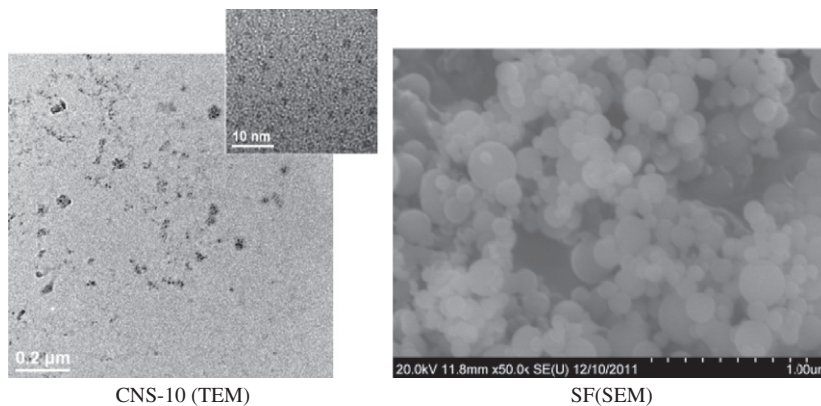

CNS-10 (TEM)   SF(SEM)

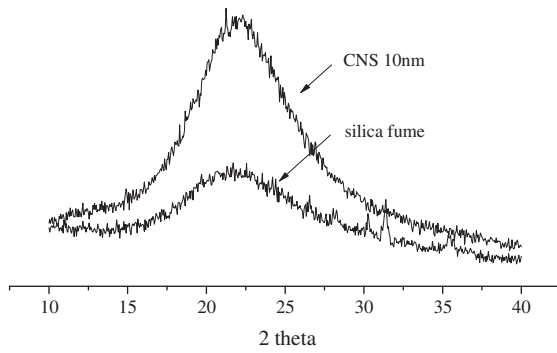**Fig. 1.** Morphology images of CNS and SF.

Fig. 2. XRD spectra of CNS and SF.

The elastic modulus of the sample can be calculated from the known properties of the indenter and the unloading part of the load – displacement curve, shown in Fig. 3. Irregular nanoindentation curves due to the presence of voids and cracking of the sample were discarded [19,20]. Statistical nanoindentation tests were carried out over three different areas of the gel phase on each sample. Over each area, 64 indents (10 μm grid point distance) were performed.

For a reliable measure of the local mechanical properties, the sample must have a flat surface [19]. In this study, samples were cast in 2 cm × 2 cm × 8 cm molds. After 1 day of casting, samples were demolded and cured in saturated lime water at room temperature. Before testing, thin sections of approximately 5 mm were cut out of the specimens and mounted on a metal sample holder

for polishing. The surface of the samples were polished using silicon carbide paper of gradation 22 μm, 14.5 μm, and 6.5 μm, and diamond lapping film of gradation 3 μm and 1 μm. Water was used for the duration of the polishing process. The polishing time was 2 min for the first 3 polishing steps and 2 h for each of the diamond polishing steps. In the final step, the polished samples were ultrasonically cleaned in water for 1 min using a bath sonicator to remove polishing debris from the sample surface. The smoothness of the sample surface was checked by SEM, as shown in Fig. 4. The root mean-squared (RMS) average roughness, obtained by Atomic Force Microscopy (AFM), for an area of 40 μm × 40 μm was 113 nm for the 5 month old control sample, which is comparable to the published data [19].

3. Results and discussions

3.1. Pozzolanic activity

To evaluate the pozzolanic activity of CNS, the CH adsorption capacity of CNS was investigated and a comparison study was made with silica fume.

It can be seen in Fig. 5 that after 7 days of hydration, the pozzolanic reaction of CNS is almost complete. However, for silica fume, it takes as long as 1 month for the completion of this reaction. Similar results can be seen in Ref. [21]. The difference in activity between CNS and SF can be due to the variation in their chemical structure: the unsaturated Si–O bonds on the CNS particle surface make the pozzolanic reaction happen quickly. However, for SF, a prior step of breaking the saturated Si–O bonds on its surface, which is relatively slow, makes the reaction slower [22]. The differ-
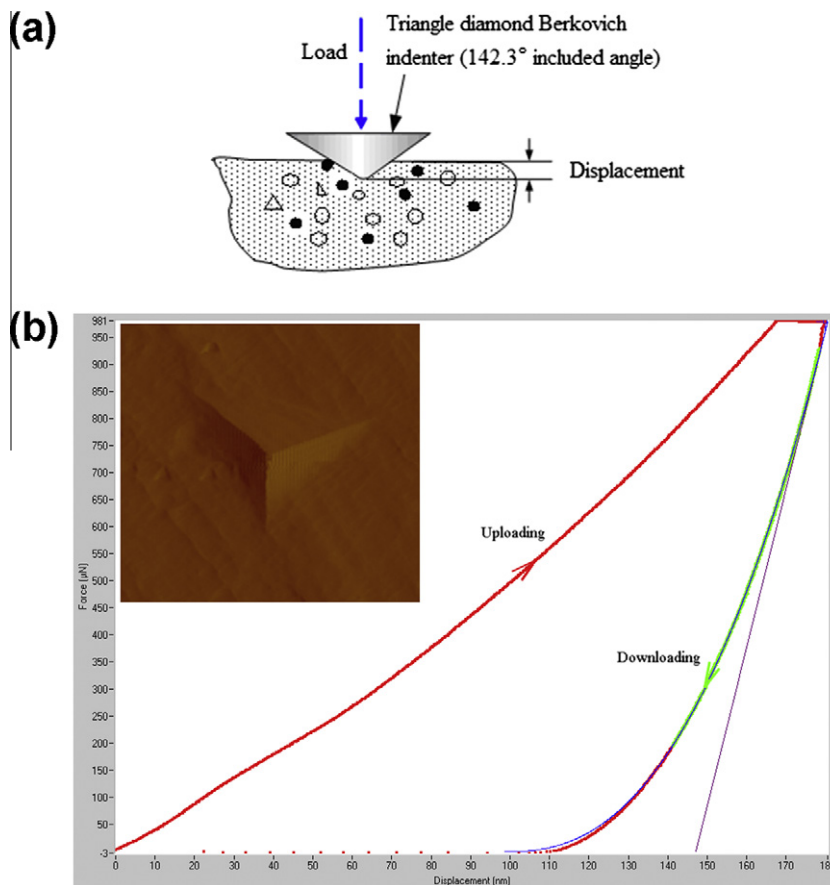

Fig. 3. Schematic diagram of nanoindentation and the typical load–displacement curve and the indent image on cement paste.
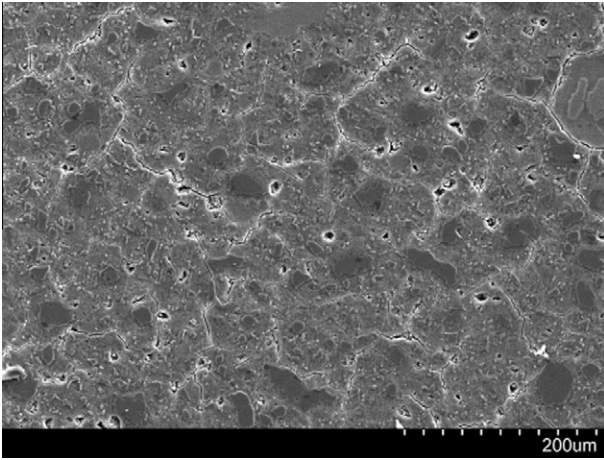
Fig. 4. Polished control sample of 5 months old.

Fig. 5. CH adsorption capability comparison of CNS and SF (w/b = 2).

Fig. 6. Strength improving effects of CNS and SF, Compressive strength ratio = $100\% \times \frac{\text{strength of mix with CNS/SF}}{\text{Strength of control mix}}$, w/b = 0.5, the fluidity of all mixes were adjusted by water reducer to achieve 210 mm.

ence in final CH consumption can be due to the difference in hydration degree of these two pozzolans. When assuming all CNS takes part in the pozzolanic reaction, a Ca/Si ratio of hydrates of 1.7 can be calculated, which is the same as plain cement paste [23].

3.2. Hydration modification

3.2.1. Strength evolution

Modification caused by the cement hydration of small particles can be reflected by their effect on the mechanical properties of cementitious materials. The strength enhancing effects of CNS and SF were measured in 40% fly ash replaced cement mortars. It is shown in Fig. 6 that CNS has a more pronounced enhancing effect in the early age: for the 5% CNS mix, compressive strength can be improved by as much as 16% and 45% at 3 and 7 days, respectively. Meanwhile, the strengths of the 5% SF mix at these ages were lower than 10%. However, the strength gain of both pozzolans in the later age are comparable. The lower compressive strength of 5% CNS-added mortar compared to the control at 84 days can be due to the hindrance of cement hydration as described in Section 3.2.4.

3.2.2. Hydration heat

The semi-adiabatic calorimetry results of the control and samples with various additions of CNS-10 and SF are shown in Fig. 7. It is clearly demonstrated that the addition of CNS increases both the hydration peak temperature and the reaction rate, the latter of which is shown by the 1st derivation of the hydration temperature curve. Similar effects can also be seen in SF-added cement pastes. It is well known that cement hydration is a dissolution-precipitation process [24] and the acceleration of this process can be monitored by the evolution of pH value and electrical conductivity (revealing the ion concentration) of the paste solution. It is shown in Fig. 8 that the addition of CNS introduces a higher rate of increase in pH and electrical conductivity in the early age (effects of CNS on pH and electrical conductivity were negligible), meaning a quicker dissolution of cement particles. The decrease in electrical conductivity is due to the adsorption of ions by the C–S–H gel and the sharper decrease exhibited by the CNS-added cement solution indicates a greater gel formation [25]. When small particles are evenly distributed in cementitious materials, they act as nucleation sites, which will benefit the hydration process [11,12,26]. The accelerated dissolving process can also be observed in SEM images, shown in Fig. 10.
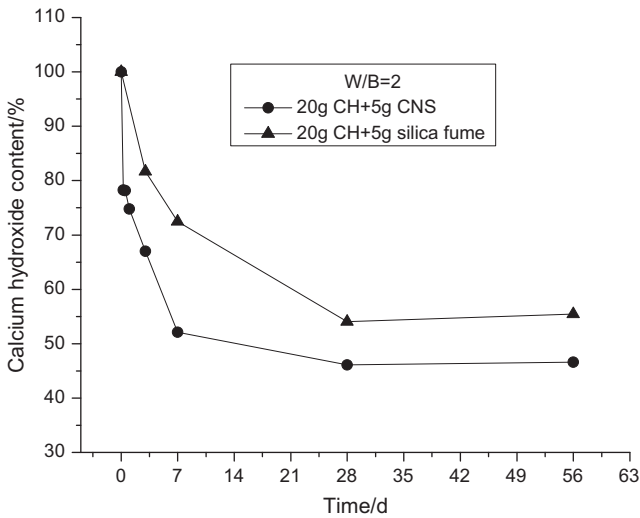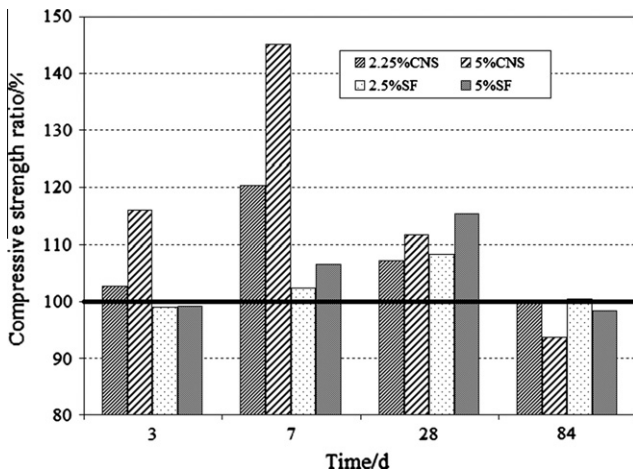
A comparison of the effect of CNS and SF on the rate of cement hydration is shown in Fig. 9. It demonstrates that CNS accelerates cement hydration at a higher rate and this can be due to the higher amount of nucleation sites, which results in a greater amount of nucleus formation [27]. However, it is also demonstrated in Fig. 9 that the hydration peak temperature of 5% SF-added paste is higher than that of CNS paste, implying a higher degree of cement hydration in SF-added paste. Similar results were shown by Thomas et al. [11], as well as some contradicting results elsewhere [6].

The degree of acceleration in hydration of small particles can be due to the effect of nucleus size on nucleation sites [27]. According to the heterogeneous nucleation theory, the nucleation free energy can be related to the volume of the solid nucleus, which can be illustrated in the following equation

$$\Delta G^* = \frac{1}{2} V^* \Delta G_V \tag{2}$$

where ΔG^* is the critical nucleation free energy, which depends on the crystalline structure and cell parameter of the nucleus and nucleation sites (assumed to be equal for CNS and SF); ΔG_V is the volume energy of solid nucleus, which depends on the particle
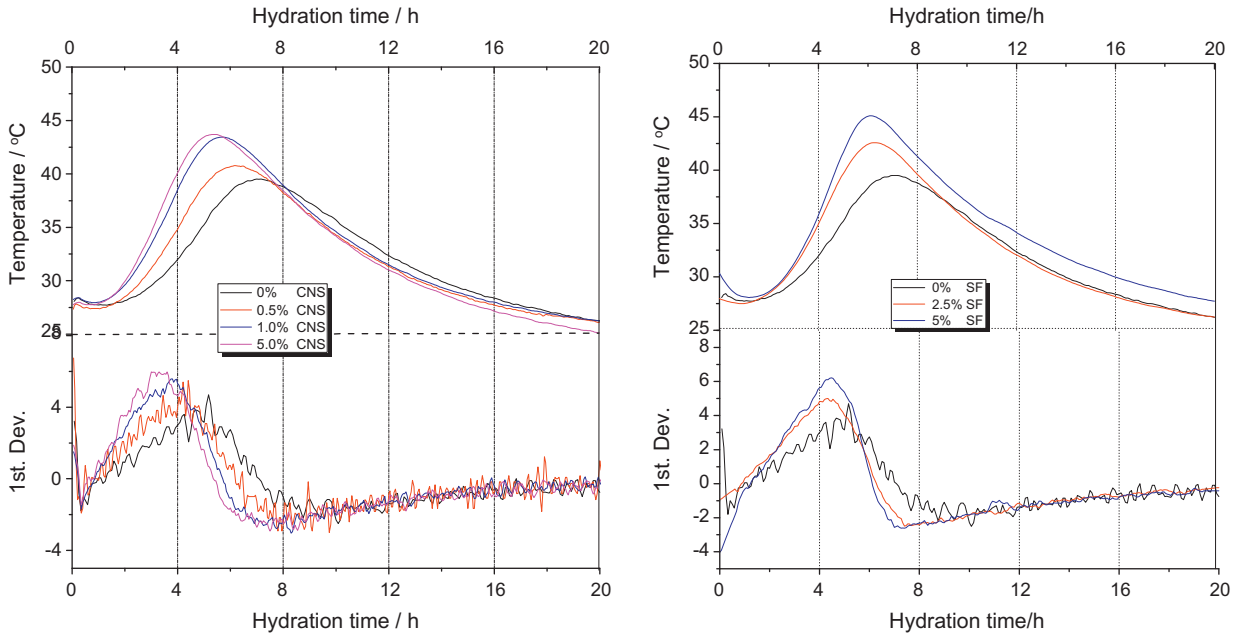
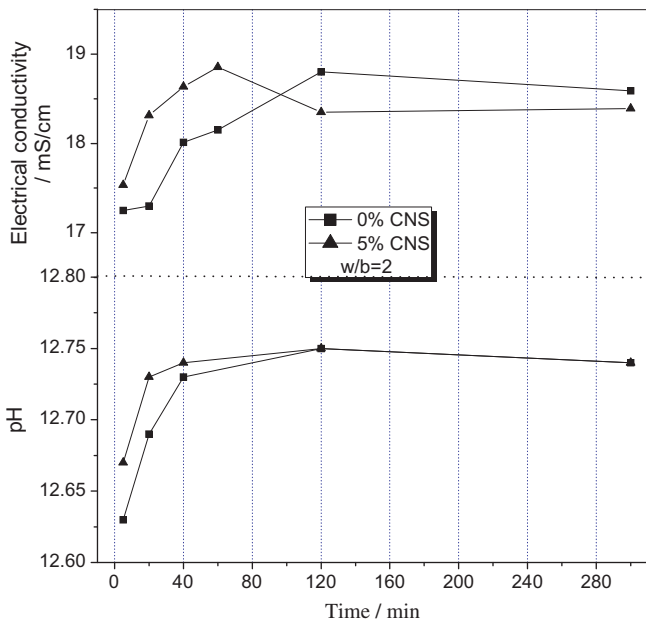**Fig. 7.** Effects of CNS and SF on cement hydration heat.

Fig. 8. Effect of CNS on pH value and electrical conductivity evolution of cement paste.
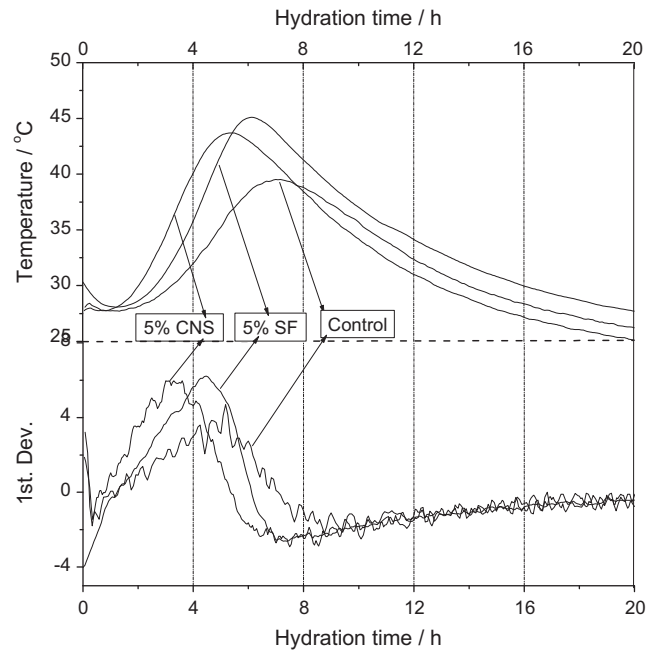

Fig. 9. Comparison of hydration acceleration effects of CNS and SF.

composition (assumed to be the same for CNS and SF); V^* is the critical volume of nucleus.

For the heterogeneous nucleation of C–S–H gel on CNS/SF surfaces, the volume of the nucleus should reach the critical volume. Although there are more nucleation sites in CNS-added paste, the probability of reaching the critical volume is lower, and thus the hydration heat can be smaller.

3.2.3. Morphology

The effect of CNS on hydration in the early age were investigated by the SEM technique (FE-SEM 4800). Noticeable changes in the appearance of the paste morphology were observed in CNS-added cement pastes.

The SEM images, Fig. 10, show the typical morphological features of cement or cement paste at various ages. Cement grains exhibit irregular shapes with flat surfaces covered by small debris. After 1 h of hydration, for the plain cement paste, there are many pits on the cement particle surface – these are due to the dissolution of the cement particle after meeting water [28]. Meanwhile, some needle-like hydrates appear on the cement particle surface. For the CNS-added paste, the surface is more seriously eroded, indicating a greater extent of dissolution. However, the characteristic needle-like hydrates are more difficult to see. A distinct feature of CNS-added paste is that the cement particles are covered with small particles that are ca. 50 nm. These can be the reacted CNS particles, which are larger than their original size of 10 nm,
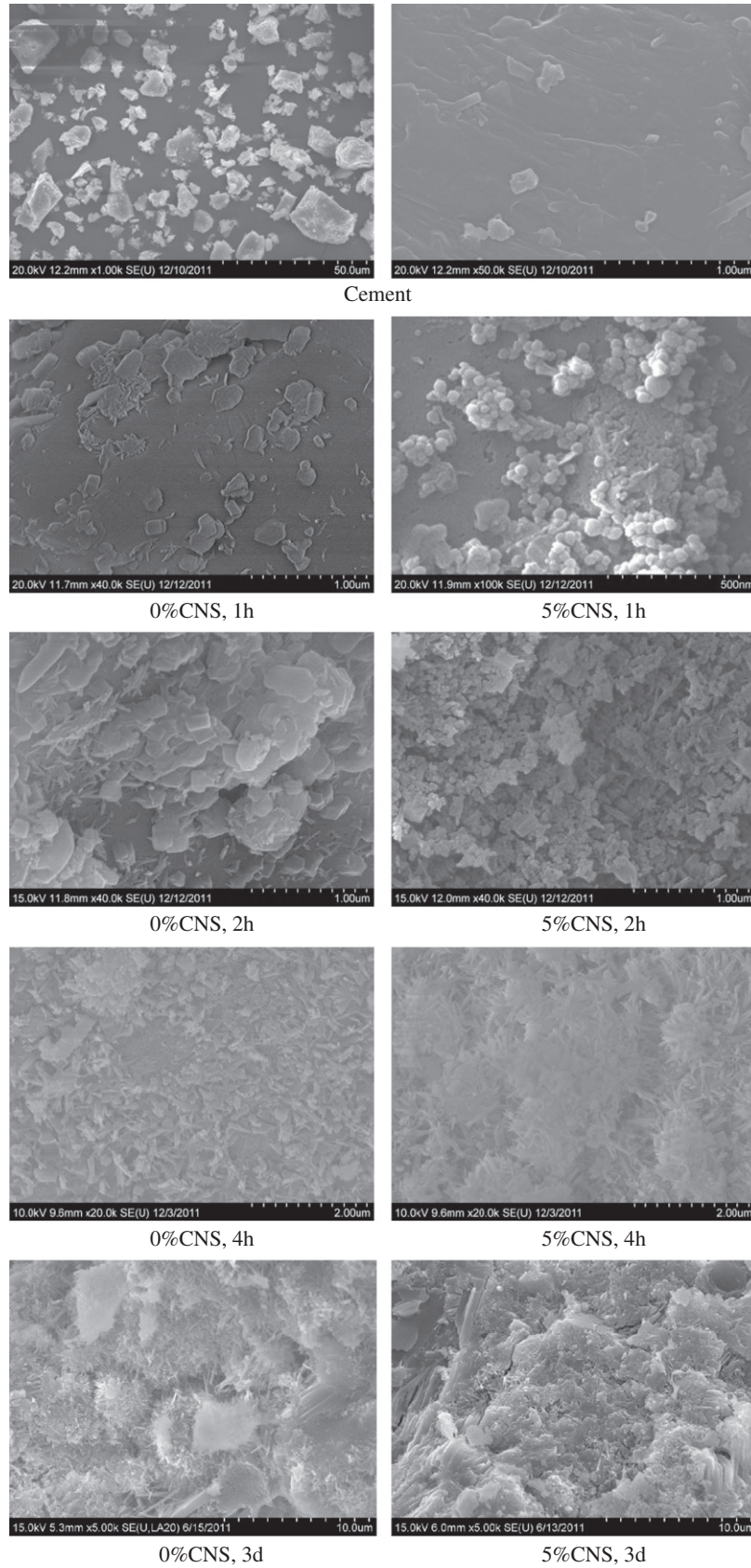
Fig. 10. SEM images of the evolution of cement at different ages.

indicating hydration of CNS. This shows that the hydration acceleration effect of CNS is achieved through the hydration of CNS. This can be supported by the hydration heat calorimetry results of CNS and C–S–H seeded pastes [11,12], the former of which shows an accelerated induction period, while, for the latter no such period occurs.

After 2 h, the control paste shows no obvious change in morphology from the 1 h old control paste due to the induction phase. However, in CNS-added paste, significant hydration can be observed: more hydrates are compacted around CNS particles and some cluster hydrates can be seen.

After 4 h, both samples are covered with immature needle-like hydration products [29]. It is apparent that the population of these products in the CNS – added paste is significantly higher than that of the control paste and the products are more compacted, as well. After 3 days of hydration, both of the pastes are characterized by the featureless and densified gel structure with amorphological CH [29]. However, it is still apparent that the CNS paste is more mature than the control paste.

The hydrate morphology evolution of CNS-added cement pastes indicates that the hydration acceleration effect of CNS is achieved by its high pozzolanic activity in the very early age, which generates C–S–H gel and then acts as nucleation sites to accelerate cement hydration. The hydration acceleration mechanism revealed by the SEM images can be verified by comparing the morphology evolution of CNS-added cement paste and of C–S–H seeded C_3S paste, as shown in Ref. [12], the latter of which shows a faster formation of new hydrates but no prior step of nucleus formation.

3.2.4. Calcium hydroxide (CH) content

Cement hydration produces CH while pozzolanic reaction consumes CH. The effect of CNS on cement hydration can be monitored by the formation of CH.

It is shown in the inserted plot of Fig. 11 that during the first 8 h of hydration, the CNS addition can increase the CH content: the CH content of 5% CNS-added paste is ca. 30% greater than that of the control paste at 4 h of hydration. A higher CH content is reached earlier than SF-added paste [30]: there is no difference in CH content between the control paste and the SF-added paste before 8 h of hydration, which reflects the higher hydration acceleration effect of CNS. The reduction in CH content in CNS-added paste afterwards is due to the pozzolanic reaction.

The effect of CNS on cement hydration can be evaluated by the difference in CH content between pastes with and without this pozzolan. This effect can be shown more apparently in the later age, during which the pozzolanic reaction has finished. The CH content disparity shown in Fig. 12 at different segments can be attributed to different reasons. Before 7 days, the pozzolanic reaction of CNS is accounted for by the CH content reduction. Although
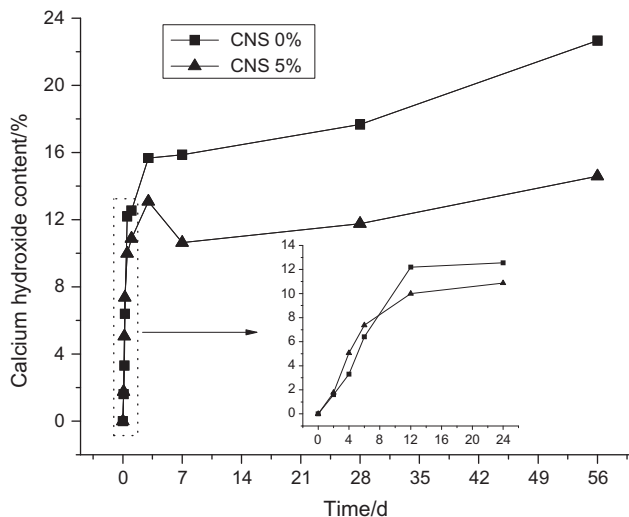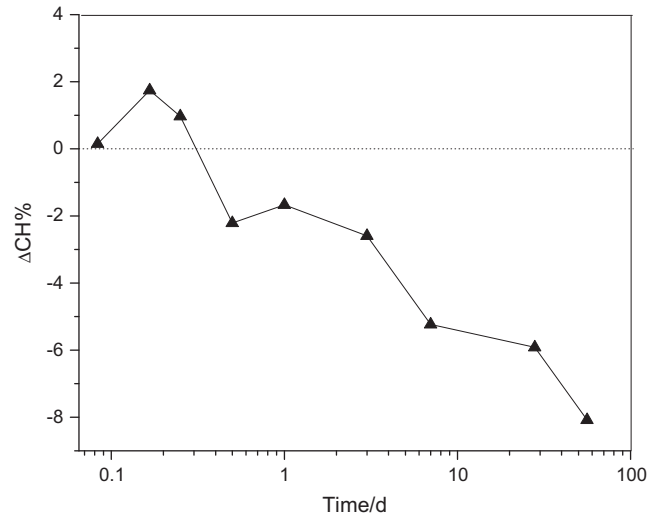

Fig. 12. CH content difference between CNS-added and control cement pastes.

the pozzolanic reaction is almost complete after 7 days (Fig. 5), the disparity in CH content keeps increasing, which implies a slowed CH generation and cement hydration of CNS-added paste in the later age. This was confirmed by the backscattered scanning electroscopic images shown in Fig. 13 (the white particles are the unhydrated cement particles). Image analysis shows that after 8 months of hydration, 96.8% cement has been reacted in control paste. However, only 89.4% took part in the reaction in 5% CNS-added paste. A coating of hydrates was observed on unhydrated cement particles of 23% CNS-added C_3S paste, which is considered to be less permeable and hinders C_3S hydration in the later age [31].

3.2.5. Non-evaporable water (NEW) content

NEW content measurement is one of the most intensively used methods of monitoring cement hydration. To quantitatively elucidate the effect of CNS-10 on the hydration of cement, NEW contents at different hydration ages were measured.

It can be seen in Fig. 14 that CNS addition has greatly changed the NEW evolution process. During the first 24 h of hydration, CNS can greatly increase the NEW content of cement paste. For example, 5% CNS addition can increase NEW content to a degree of about 50% at 4 h. However, after 3 days, NEW content of CSN – added paste becomes lower than that of the control. Two months later, the NEW content of 5% CNS – added paste is 10% lower that the control paste.

A similar phenomenon was observed in SF-added cement paste. It is shown in Fig. 15 that before 28 days of hydration, SF addition increases the NEW content. However, the NEW content of SF– added paste becomes lower than the control after 1 month.

As the pozzolanic reaction is a water-intake process other than that from CH [32], the decrease in NEW content can be due to gel structure modification. Gaitero [3] used the ^{29}Si MAS–NMR technique to study the silicate tetrahedron evolution of cement paste and showed that the mean chain length of 0% and 8% nano-SiO_2-added gels were 2.9 and 3.5, respectively. During the polymerization process (Eq. (3)), combined water in silicate chains can be released, resulting in a decrease of NEW content of the paste [30].

$$(Si_2O_7)^{6-} + (Si_2O_7)^{6-} = (Si_4O_{13})^{10-} + H_2O \qquad (3)$$
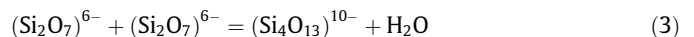
From the discussion, it is known that NEW measurement is not valid for monitoring the hydration of cement pastes with pozzolanic materials such as CNS and silica fume [27]. This was also found in
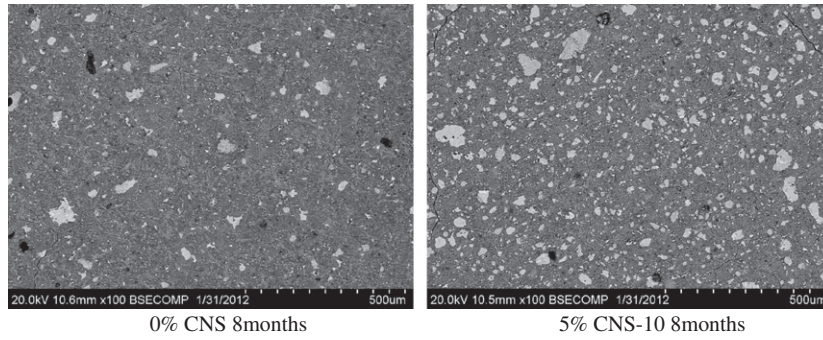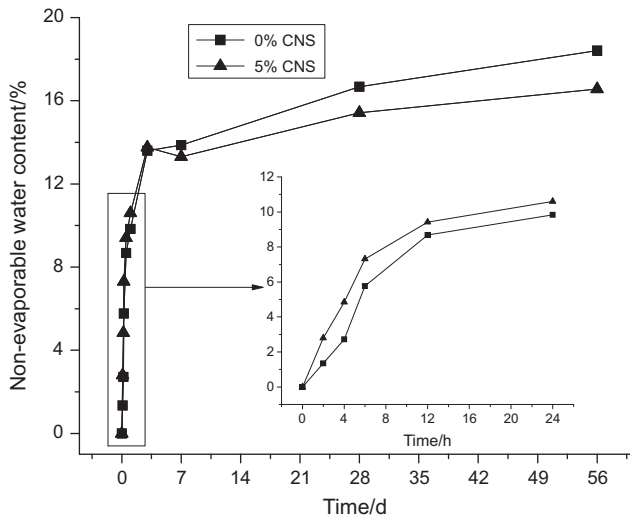

Fig. 11. Effect of CNS-10 nm on CH content of cement paste.

0% CNS 8months 5% CNS-10 8months

Fig. 13. BSE images of cement pastes.

Fig. 14. Effect of CSN on NEW content of cement paste.

Fig. 15. Effect of SF on NEW content of cement paste.

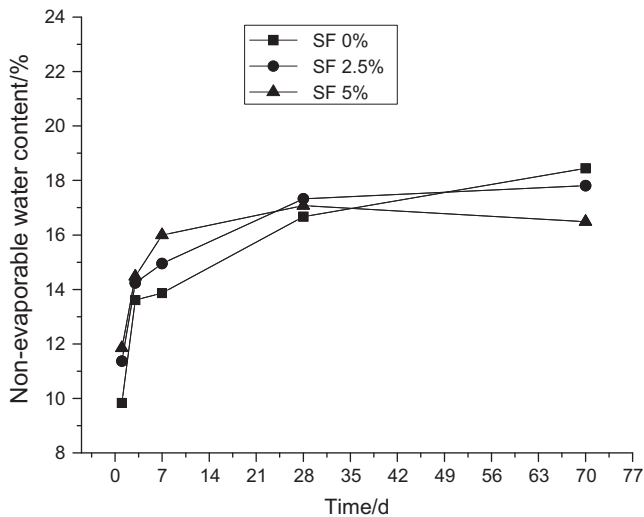**Fig. 16.** Effect of CNS on the elastic modulus of cement paste.

cementitious materials, Therefore its nanoscale mechanical properties were investigated.

3.3. Nanoscale mechanical property

Studies have shown that the nanoscale mechanical properties of C–S–H gel are intrinsic properties. For plain cement paste, five different phases are determined by the grouping of the elastic modulus, which are porous phase (ca. 0–10 GPa), low-stiffness (ca. 10–25 GPa) and high-stiffness (ca. 25–35 GPa) C–S–H gel, calcium hydroxide (ca. 35–45 GPa) and clinker (>45 GPa) [35].

To evaluate the effect of CNS on the gel properties, the elastic modulus of the 5 month old cement paste with and without 5% CNS-10 were measured and are shown in Fig. 16. In this graph, data smaller than 10 GPa or higher than 50 GPa, which are attributed to porous and clinker phases, are excluded in the analysis.

It can be seen in Fig. 16 that for the plain paste, the main peak of the elastic probability plot falls in the low-stiffness gel region (ca. 10–25 GPa). When CNS was added, the high-stiffness gel region is more pronounced, which indicates an increase in high-stiffness C–S–H gel. When taking the degree of cement hydration into consideration, shown in Fig. 13, it is evident that the increase in high-stiffness gel is caused by the pozzolanic reaction of CNS. An increase in high-stiffness C–S–H gel content was also observed in

high volume fly ash cementitious materials system [33,34]. And the lower NEW content of the CNS-added paste compared to the control early on may indicate an earlier occurrence of the average silicate chain elongation.

From this it can be deduced that the effect of CNS on gel properties can be a critical factor in influencing the properties of

carbon-nanotube-incorporated cementitious material [36]. Gaitero [3] and Mondal [19] compared the nanoindentation results of 6% and 18% CNS-added pastes and found that the latter has a higher proportion of the high-stiffness C–S–H gel, which shows a consistent trend with the present results. An obvious reduction in CH content in the 5% CNS paste, shown by the reduction in the area of the modulus region 35–45 GPa, can be due to the pozzolanic reaction of CNS.

Gaitero [3] reported that high-stiffness C–S–H is more resistant to calcium leaching, thus the addition of nanosilica has a positive impact on durability.

4. Conclusions

Effects of nano-SiO$_2$ on the cement hydration process, as well as its influence on the gel structure and nanoscale mechanical properties of cement paste were studied. Results showed that:

(1) Pozzolanic activity of colloidal nanoSiO$_2$ is higher than that of silica fume and its hydration acceleration effect is also higher than silica fume in the early age, but this effect is comparable to that of silica fume in the later age;
(2) Acceleration of cement hydration and maturation of gel structure in CNS-added paste is achieved through an acceleration of the dissolution of cement particles and a preferred hydration and hydrates precipitation on CNS particle surface. Although CNS can accelerate cement hydration to a great extent in the early age, the later hydration of cement is hindered;
(3) NEW content measurement is not suitable for monitoring the hydration process of CNS-added paste, which in the later age will gradually decrease due to the effect of CNS on the gel structure;
(4) A reduction in low-stiffness C–S–H gel and an increase in high-stiffness C–S–H gel can be the result of CNS addition.

Acknowledgements

References

[1] Sobolev K, Shah SP. Nanotechnology of concrete: recent developments and future perspectives. ACI Mater J 2008 [special publication].
[2] Collepardi M, Collepardi S, Skarp U, et al. Optimization of silica fume, fly ash and amorphous nano-silica in superplasticized high-performance concretes. In: Proceedings of 8th CANMET/ACI international conference on fly ash, silica fume, slag and natural pozzolan in concrete SP221 USA, vol. 30; 2004. p. 495–506.
[3] Gaitero JJ. Multi-scale study of the fiber-matrix interface and calcium leaching in high performance concrete. Ph.D thesis, Labein-Technalia, Spain; 2008.
[4] Ali Nazari, Shadi Riahi. The effects of SiO$_2$ nanoparticles on physical and mechanical properties of high strength compacting concrete. Composites Part B 2011;42(3):570–8.
[5] Said AM, Zeidan MS. Enhancing the reactivity of normal and fly ash concrete using colloidal nano-silica. ACI Mater J 2009;267:75–86 [special publication].
[6] Jo BW, Kim CH, Tae G, et al. Characteristics of cement mortar with nano-SiO$_2$ particles. Constr Build Mater 2007;21(6):1351–5.
[7] Li H, Xiao H, Yuan J, et al. Microstructure of cement mortar with nano-particle. Composites Part B 2004;35(2):185–9.
[8] Gundogdu D, Pekmezci BY, Atahan HN. Influence of nanosilica on the mechanical properties of mortars containing fly ash. In: Brameshuber E, editor. International RILEM conference on material science-AdIPoC-additions improving properties of concrete (AdIPoC). RILEM Publications SARL; 2010; p. 345–54.
[9] Gaitero JJ, Campillo I, Guerrero A. Reduction of the calcium leaching rate of cement paste by addition of silica nanoparticles. Cem Concr Res 2008;38(8–9):1112–8.
[10] Shih JY, Chang TP, Hsiao TC. Effect of nanosilica on characterization of Portland cement composite. Mater Sci Eng A 2006;424:266–74.
[11] Thomas JJ, Jennings HM, Chen JJ. Influence of nucleation seeding on the hydration mechanisms of tricalcium silicate and cement. J Phys Chem 2009;113(11):4327–34.
[12] Alizadeh R, Raki L, Makar JM, et al. Hydration of tricalcium silicate in the presence of synthetic calcium-silicate-hydrate. J Mater Chem 2009;19:7937–46.
[13] Lu P, Sun G, Young JF. Phase Composition of hydrated DSP cement pastes. J Am Ceram Soc 1993;76(4):1003–7.
[14] Yajun J, Cahyadi JH. Simulation of silica fume blended cement hydration. Mater Struct 2004;37:397–404.
[15] Sanchez F, Sobolev K. Nanotechnology in concrete – a review. Constr Build Mater 2010;24:2060–71.
[16] Quercia G, Hüsken G, Brouwers HJH. Water demand of amorphous nano silica and its impact on the workability of cement paste. Cem Concr Res 2012;42:344–57.
[17] <http://www.mknano.com/item-details.asp?catDisp=2&itemid=80&id=10>. MK Impex Corporation, Canada.
[18] Lam L, Yong YL, Poon CS. Degree of hydration and gel/space ratio of high-volume fly ash/cement systems. Cem Concr Res 2000;34:1541–7.
[19] Mondal P. Nanomechanical properties of cementitious materials. PhD thesis, Northwestern University, USA; 2008.
[20] Wang XH, Jacobsen S, He JY, et al. Application of nanoindentation testing to study of the interfacial transition zone in steel fiber reinforced mortar. Cem Concr Res 2009;39(8):701–15.
[21] Wu Z, Young JF. The hydration of tricalcium silicate in the presence of colloidal silica. J Mater Sci 1984;19:3477–86.
[22] Ye Q, Zhang Z, Kong D, et al. Influence of nano-SiO$_2$ addition on properties of hardened cement paste as compared with silica fume. Construct Build Mater 2007;21:539–45.
[23] Escalante-Garcia JI, Mendoza G, Sharp JH. Indirect determination of the Ca/Si ratio of the C–S–H gel in Portland cements. Cem Concr Res 1999;29:1999–2003.
[24] Scrivener KL, Nonat A. Hydration of cementitious materials, present and future. Cem Concr Res 2011;41:651–65.
[25] Morsy MS. Effect of temperature on electrical conductivity of blended cement pastes. Cem Concr Res 1999;29:603–6.
[26] Land G, Stephan D. The influence of nano-silica on the hydration of ordinary Portland cement. J Mater Sci 2012;47:1011–7.
[27] Givi AN, Rashid SA, Aziz FN, et al. Experimental investigation of the size effects of SiO$_2$ nano-particles on the mechanical properties of binary blended concrete. Composites Part B 2010;41:673–7.
[28] Ylmén R, Jäglid U, Steenari B, et al. Early hydration and setting of Portland cement monitored by IR, SEM and Vicat techniques. Cem Concr Res 2009;39(5):433–9.
[29] Diamond S. Cement paste microstructure – an overview at several levels. Hydraulic cement pastes: their structure and properties. In: Proceedings of the conference on Hydraulic Cement Pastes. University of Sheffield, Sheffield; April, 1976. p. 2–29.
[30] Huang C, Feldman RF. Hydration reactions in Portland cement-silica fume blends. Cem Concr Res 1985;15(4):585–92.
[31] Thomas J, Jennings H. The nanostructure of low-CO$_2$ concrete for a sustainable infrastructure. Report on year 1 activities and recommendations for future work, A scientific collaboration between Lafarge Center for Research (LCR) and Northwestern University (NWU); 2010.
[32] Escalante-Garcia JI. Nonevaporable water from neat OPC and replacement materials in composite cements hydrated at different temperatures. Cem Concr Res 2003;33:1883–8.
[33] Zhang Y, Sun W, Yan HD. Hydration of high-volume fly ash cement pastes. Cem Concr Compos 2000;22(6):445–52.
[34] James Kirkpatrick R. Nuclear magnetic resonance spectroscopy. In: Ramachandran VS, Beaudoin JJ, editors. Handbook of analytical techniques in concrete science and technology principles, techniques, and applications. Ottawa, Canada; 2001.
[35] Constantinides G, Ulm FJ. The nanogranular nature of C–S–H. J Mech Phys Solids 2007;55(1):64–90.
[36] Konsta-Gdoutos MS, Metaxa ZS, Shah SP. Multi-scale mechanical and fracture characteristics and early-age strain capacity of high performance carbon nanotube/cement nanocomposites. Cem Concr Compos 2010;32(2):110–5.